Retrieval of Moisture from Simulated GPS Slant-path Water Vapor Observations using 3DVAR with Anisotropic Recursive Filters

Haixia Liu[1,2], Ming Xue[1,2], R. James Purser[3] and David F. Parrish[4]

[1]Center for Analysis and Prediction of Storms and [2]School of Meteorology
University of Oklahoma, Norman OK 73019

[3]Science Applications International Corporation, Beltsville, Maryland

[4]Environmental Modeling Center, National Centers for Environmental Prediction
Camp Springs, MD 20746-4304

[*]Corresponding Author Address:
Dr. Ming Xue
School of Meteorology
University of Oklahoma
100 E. Boyd
Norman OK 73019
mxue@ou.edu

Abstract

Anisotropic recursive filters are implemented within a three-dimensional variational (3DVAR) framework to efficiently model the effect of flow-dependent background error covariance. The background error covariance is based on an estimated error field and on the idea of Riishøjgaard. In the anisotropic case, the background error pattern can be stretched or flattened in directions oblique to the alignment of the grid coordinates and is constructed by applying at each point six recursive filters along six directions corresponding, in general, to a special configuration of oblique lines of the grid. The recursive filters are much more efficient than corresponding explicit filters used in an earlier study and are therefore more suitable for real time numerical weather prediction.

A set of analysis experiments are conducted at a mesoscale resolution to examine the effectiveness of the 3DVAR system in analyzing simulated Global Positioning System (GPS) slant-path water vapor observations from ground-based GPS receivers and observations from collocated surface stations. It is shown that the analyses produced with recursive filters are at least as good as those with corresponding explicit filters. In some cases, the recursive filters actually perform better.

The impact of flow-dependent background errors modeled using the anisotropic recursive filters is also examined. The use of anisotropic filters improves the analysis, especially in terms of fine-scale structures. The analysis system is found to be effective in the presence of typical observational errors. The sensitivity of isotropic and anisotropic recursive-filter analyses to the de-correlation scales is also examined systematically.

1. Introduction

The poor knowledge of fine-scale spatial and temporal distributions of water vapor is partly responsible for the slow improvement in quantitative precipitation forecasts (QPF). The International H_2O Project (IHOP, 13 May through 25 June 2002, Weckwerth et al. 2004), was conducted over the central Great Plains of the United States to investigate, as one of its goals, the four-dimensional distribution of atmospheric water vapor and its impact on QPF. During IHOP_2002, a network of sensors collected numerous water vapor data. This network included ground-based GPS receivers which measure the delay along the slant path from GPS satellites to the ground-based receivers. The total integrated water along the slant paths can be derived from the slant-path wet delay (the part of the delay caused by the water vapor) (Rocken et al. 1993; Ware et al. 1997; Braun et al. 2001).

Due to the integrated nature of the GPS observations, a variational method is the natural choice for analyzing such data. Most of the earlier work utilizing variational methods examined the impact of the vertically integrated water vapor, or precipitable water (*PW*), or the zenith total delay (*ZTD*) data (Kuo et al. 1993; 1996; Guo et al. 2000; De Pondeca and Zou 2001a; 2001b; Falvey and Beavan 2002; Cucurull et al. 2004). Despite the fact that they all found a positive impact of assimilating the GPS data on short-range (within 6 hours) precipitation forecasts for their specific cases, there is a loss of information content when using derived *ZTD* or *PW* data as compared to the original slant-path data, due to the spatial and temporal averaging involved in their derivation. It should, therefore, be beneficial to exploit the slant-path total or wet delay or slant-path water vapor (*SWV*) data directly. The multiple slant paths form, in a sense, a 'net', that provides a much better three-dimensional (3D) coverage than the vertical-only zenith paths. Further discussions on the GPS data in various forms can be found in Liu and Xue (2006,

hereafter abbreviated as LX06). So far, there has been only a very limited number of studies that directly analyze slant-path data (MacDonald et al. 2002; Ha et al. 2003; Liu and Xue 2006), all utilizing simulated data from hypothetical GPS networks. These works demonstrated the effectiveness of variational procedures in recovering 3D moisture structures from slant-path water vapor observations.

Many efforts have been made to develop more accurate GPS observation operators to reproduce the slant measurements; most variational analysis systems, however, still assume isotropic and static background error statistics. For slant-path GPS data, MacDonald et al. (2002) did not use a model background term. Ha et al. (2003) assumed the background error covariance is diagonal in their four-dimensional variational (4DVAR) system. It is well known that flow-dependent background error covariance (some times called the 'error of the day' for large scale applications, see, e.g., Pu et al. 1997) plays an important role in data assimilation. Such an error covariance is usually spatially inhomogeneous and anisotropic. The background error covariance builds the relationship between the grid points and determines how the observation innovations are spread in the analysis domain. Consequently, the reliable estimation of the degrees and orientations of anisotropy in the moisture background errors is important for moisture analysis and QPF forecasts because of the high spatial variability in moisture.

In our recent study (LX06), a 3D variational (3DVAR) analysis system is developed that models the flow-dependent background error field using an explicit spatial filter. Better moisture analysis from simulated GPS slant-path water vapor data is obtained when using an anisotropic spatial filter to model the flow-dependent background error covariance. The explicit anisotropic filter, when applied over even a moderate number of grid points in three dimensions, is, however, too expensive in terms of both computational and memory storage costs, because of the

need to calculate and store filter coefficients locally and apply the filter explicitly at every grid point, in all three directions. A much more computationally efficient algorithm is the implicit recursive filter, whose flow-dependent anisotropic version, though much more complex than the isotropic version, has seen significant development recently (Purser et al. 2003a, b). The significantly increased efficiency using recursive filters makes their implementation in operational data assimilation systems practical.

In this paper, the recursive filter with an anisotropic option is implemented in our 3DVAR system. Some retrieval experiments of GPS slant-path water vapor data are performed and the results are compared with those of explicit filters reported in LX06. We also examine the impact of flow-dependent background errors realized through anisotropic recursive filters on the quality of 3DVAR analysis. Further, the sensitivity of isotropic and anisotropic recursive-filter analyses to the spatial de-correlation scales is also examined systematically. We point out here that even though the experiments performed in this paper are similar to those presented in LX06, the implementation of anisotropic recursive filters for the modeling of truly flow-dependent background error structures represents significant progress. The use of experiments with very similar configurations as those in LX06 facilitates the comparison with the results of explicit filters.

The rest of this paper is organized as follows. Section 2 describes our 3DVAR system and a scheme for determining flow-dependent background error covariances. It also describes the procedure for determining the recursive filter coefficients, especially for the anisotropic case, given the modeled background error covariances. Section 3 introduces our hypothetical ground-based GPS observation network and the simulation of GPS slant-path data. After illustrating in section 4 the effect of recursive filters on the analyses with single observation tests, we apply in

section 5 our 3DVAR system to the 3D moisture retrieval. In section 6, we check the effect of filter length scales on the analysis quality and the sensitivity of the analysis to observational errors. Conclusions are given in section 7, together with suggested future work.

2. 3DVAR system with recursive filters

We present in this section the 3DVAR analysis system developed and used in this study. It is based on the 3DVAR system developed by LX06. It uses a preconditioner that involves the square root of the background error covariance matrix, **B**, instead of **B** itself as in LX06. As a result, the control variables of the current incremental 3DVAR system are different from those used in LX06. Further, it uses a recursive filter instead of an explicit spatial filter to model **B**. The notation of Ide et al. (1997) is used in the equations below.

a. 3DVAR cost function

A variational method is to find an analysis that minimizes a predefined cost function. In this study, the cost function is defined as,

$$J(\mathbf{x}) = J_b(\mathbf{x}) + J_{swv}(\mathbf{x}) + J_{sfc}(\mathbf{x}) + J_c(\mathbf{x}), \tag{1}$$

where,

$$J_b(\mathbf{x}) = \frac{1}{2}(\mathbf{x} - \mathbf{x}_b)^T \mathbf{B}^{-1}(\mathbf{x} - \mathbf{x}_b), \tag{2a}$$

$$J_{swv}(\mathbf{x}) = \frac{1}{2}\left[H_{swv}(\mathbf{x}) - \mathbf{SWV}\right]^T \mathbf{R}_{swv}^{-1}\left[H_{swv}(\mathbf{x}) - \mathbf{SWV}\right], \tag{2b}$$

$$J_{sfc}(\mathbf{x}) = \frac{1}{2}\left[H_{sfc}(\mathbf{x}) - \mathbf{q}_{v_{sfc}}\right]^T \mathbf{R}_{sfc}^{-1}\left[H_{sfc}(\mathbf{x}) - \mathbf{q}_{v_{sfc}}\right], \tag{2c}$$

$$J_c(\mathbf{x}) = \frac{1}{2}\left(\frac{\mathbf{x} - |\mathbf{x}|}{2}\right)^T W_c\left(\frac{\mathbf{x} - |\mathbf{x}|}{2}\right). \tag{2d}$$

In the above equations, superscript '*T*' denotes matrix transpose. The cost function *J* given in Eq. (1) is composed of four terms. The first is the background term, defined in (2a), and the second and third, (2b) and (2c), are, respectively, the observational terms for GPS *SWV* and regular surface moisture observations. The physical requirement that water vapor is nonnegative

is expressed in the last term, (2d), as a weak constraint. The operational NCEP SSI analysis (Parrish and Derber 1992) also uses a weak constraint, but on relative humidity being positive and not supersaturated (Derber, personal communication, 2006). Being a weak constraint, it does not strictly enforce the positivity of the analyzed water vapor field, however. The definitions of the variables in the equations are given as follows.

$\mathbf{x}$ is the analysis or control variable vector, which in our case is the 3D specific humidity field.

$\mathbf{x}_b$ is the analysis background or first guess, of specific humidity in this case.

$\mathbf{q}_{v_{sfc}}$ is the surface observation vector of specific humidity.

$\mathbf{B}$ is the background error covariance matrix. This study focuses on the effect of $\mathbf{B}$ in isotropic and anisotropic forms on the analysis. Assuming the background error variances are homogeneous, i.e., equal to a constant in the analysis domain, then $\mathbf{B}$ is the product of this constant and background error correlation matrix.

$\mathbf{SWV}$ is a vector containing *SWV* observations.

H_{swv} is the forward observation operator which calculates integrated *SWV* observations between GPS satellites to ground-based receivers from water vapor values at grid points.

H_{sfc} is the forward observation operator for surface observations of specific humidity.

$\mathbf{R}_{swv}$ and $\mathbf{R}_{sfc}$ are, respectively, the observation error covariances for *SWV* and surface moisture observations. The observation errors are assumed to be uncorrelated, therefore the error covariances are diagonal. Usually, the diagonal elements of $\mathbf{R}_{swv}$ ($\mathbf{R}_{sfc}$) are the *SWV* (surface moisture) observation error variances which are assumed here to be independent of stations, so $\mathbf{R}_{swv}$ ($\mathbf{R}_{sfc}$) can be simplified as a constant error variance multiplying an identity matrix, i.e., $\mathbf{R}_{swv} = \sigma^2_{swv}\mathbf{I}$ and $\mathbf{R}_{sfc} = \sigma^2_{sfc}\mathbf{I}$.

W_c is the weighting coefficient (a scalar) for nonnegative weak constraint.

Given that $\mathbf{R}_{swv} = \sigma_{swv}^2 \mathbf{I}$ and $\mathbf{R}_{sfc} = \sigma_{sfc}^2 \mathbf{I}$, the $\mathbf{R}_{swv}^{-1}$ and $\mathbf{R}_{sfc}^{-1}$ in Eqs.(2b) and (2c) can be replaced by σ_{svw}^{-2} and σ_{sfc}^{-2}, respectively, or by $W_{swv} = \sigma_{swv}^{-2}$ and $W_{sfc} = \sigma_{sfc}^{-2}$, which we call the weighting coefficients for the SWV and surface observation terms. Similarly, the background term in Eq.(2a) is proportional to a weighting coefficient, W_b, that is equal to the inverse of the background error variance, i.e., $W_b = \sigma_b^{-2}$ (see more discussion later).

In this study, except for one experiment, the simulated data are assumed error-free, i.e., no error is added to the simulated observations. This assumption, as in LX06, allows us to determine how well, under an idealized error-free condition, a 3DVAR procedure as developed here can retrieve the 3D structure of the moisture field from the slant-path water vapor data, which are integrated quantities along the slant paths rather than local observations. The answer to this question was not obvious before our first study (LX06). This error-free assumption is kept in this study for most experiment to facilitate direction comparisons of the results with those of LX06.

Theoretically, the weighting coefficients of the observation terms should be infinitely large when the observations are error-free, which means the elimination of background and its constraint term in the cost function because of the relative magnitudes of the terms. Without the background term, our analysis problem is under-determined. To retain the effect of the background term, in particular, the structure information contained in the background error covariance, we choose relative weights of 1, 100, 500 and 50 for the four terms in the cost function. The much higher weights given to the observation terms reflect the much higher accuracy of the observations as compared to the background, and the differences in the weights are sufficiently large to ensure a close fit of the analysis to the observations. Here the surface

observations are given more weight because they tend to be more accurate. A different set of weights will be used for one experiment (UB_err, see Table 1) in which observations contain errors. Finally, we point out that it is the spatial structure of the background error correlation that determines the spatial spread of the observation information (see, e.g., Kalnay 2002); the small weight of the background term does not diminish this role.

Usually, the dimensionality of matrix $\mathbf{B}$ is too large to directly compute or store in its entirety. To avoid the inversion of $\mathbf{B}$ and to improve the conditioning of the minimization problem, a new control variable, $\mathbf{v}$, is defined which satisfies

$$\delta \mathbf{x} = \mathbf{D}\mathbf{v},$$ (3)

where $\delta \mathbf{x} \equiv \mathbf{x} - \mathbf{x}_b$ is the increment of $\mathbf{x}$, and $\mathbf{D}$ is defined as $\mathbf{D}\mathbf{D}^T = \mathbf{B}$.

The cost function, J, can then be rewritten as,

$$
\begin{aligned}
J(\mathbf{v}) = \frac{1}{2}\mathbf{v}^T\mathbf{v} &+ \frac{1}{2}\left[H_{swv}\left(\mathbf{x}_b + \mathbf{D}\mathbf{v}\right) - \mathbf{SWV}\right]^T \mathbf{R}_{swv}^{-1}\left[H_{swv}\left(\mathbf{x}_b + \mathbf{D}\mathbf{v}\right) - \mathbf{SWV}\right] \\
&+ \frac{1}{2}\left[H_{sfc}\left(\mathbf{x}_b + \mathbf{D}\mathbf{v}\right) - \mathbf{q}_{v_{sfc}}\right]^T \mathbf{R}_{sfc}^{-1}\left[H_{sfc}\left(\mathbf{x}_b + \mathbf{D}\mathbf{v}\right) - \mathbf{q}_{v_{sfc}}\right] \\
&+ \frac{1}{2}\left[\frac{\mathbf{x}_b + \mathbf{D}\mathbf{v} - |\mathbf{x}_b + \mathbf{D}\mathbf{v}|}{2}\right]^T W_c\left[\frac{\mathbf{x}_b + \mathbf{D}\mathbf{v} - |\mathbf{x}_b + \mathbf{D}\mathbf{v}|}{2}\right].
\end{aligned}
$$ (4)

This new cost function contains no inverse of $\mathbf{B}$ and the conditioning of the cost function is improved by this variable transformation. The iterative minimization algorithm used in this study is the LBFGS method (Liu and Nocedal 1989). The implementation of this (as well as most other) minimization method requires that the gradient of the cost function $J(\mathbf{v})$ be evaluated with respect to the control variable $\mathbf{v}$. The gradient $\nabla_{\mathbf{v}} J$ is given by differentiating J in Eq. (4) with respect to $\mathbf{v}$ as follows,

$$\nabla_{\mathbf{v}} J = \mathbf{v} + \mathbf{D}^T\mathbf{H}_{swv}{}^T\mathbf{R}_{swv}^{-1}\left(\mathbf{H}_{swv}\mathbf{D}\mathbf{v} - \mathbf{d}_{swv}\right) + \mathbf{D}^T\mathbf{H}_{sfc}{}^T\mathbf{R}_{sfc}^{-1}\left(\mathbf{H}_{sfc}\mathbf{D}\mathbf{v} - \mathbf{d}_{sfc}\right) + \nabla_{\mathbf{v}} J_c,$$ (5)

where $\mathbf{H}_{swv}$ and $\mathbf{H}_{sfc}$ are the linearized perturbation operators of the observation operator H_{swv} and H_{sfc}; $\mathbf{d}_{swv}$ and $\mathbf{d}_{sfc}$ are the innovation vectors of SWV and surface moisture observations which are given respectively by $\mathbf{d}_{swv} = \mathbf{SWV} - H_{swv}(\mathbf{x}_b)$, $\mathbf{d}_{sfc} = \mathbf{q}_{v_{sfc}} - H_{sfc}(\mathbf{x}_b)$, and $\nabla_\mathbf{v} J_c$ is given by $\nabla_\mathbf{v} J_c = W_c \mathbf{D}^T (\mathbf{x}_b + \mathbf{Dv})$ which is only applied when the analyzed moisture, typically of the previous iteration, is negative. In all experiments presented in this paper, the recursive filter models matrix $\mathbf{D}$ and is applied to control variable $\mathbf{v}$. No explicit background error covariance matrix is involved in the calculation of the cost function or its gradient.

As discussed earlier, the background error covariance controls the extent to which values at the grid points away from an observation are influenced by the observation innovation. The effect of this covariance can be modeled using a spatial filter (Huang 2000) as follows,

$$b_{ij} = \sigma_b^2 \exp\left[-\frac{1}{2} \left(\frac{r_{ij}}{L_r} \right)^2 \right] \equiv \sigma_b^2 C_{ij}, \tag{6}$$

where r_{ij} is the 3D distance between two grid points i and j measured in terms of the grid index coordinate, L_r is the *geometric* de-correlation length scale in terms of the grid intervals and is in practice often linked to the observation density. σ_b^2 is the background error variance, which we assume to be constant, and C_{ij} is the background error correlation coefficient between the ith and j^{th} points. **66**This definition in Eq. (**66**) provides an isotropic background error covariance because the spatial correlation only depends on the distance, not direction. If L_r is constant, then the covariance is also spatially homogeneous. With the covariance defined by Eq.(6) or later by Eq.(**7**) and constant σ_b^2, the background error covariance matrix can be written as $\mathbf{B} = \sigma_b^2 \mathbf{C}$ where $\mathbf{C}$ is the correlation coefficient matrix made up of C_{ij}.

An alternative to Eq. (6) is the following anisotropic covariance,

$$b_{ij} = \sigma_b^2 \exp\left[-\frac{1}{2}\left(\frac{r_{ij}}{L_r} \right)^2 \right] \exp\left[-\frac{1}{2}\left(\frac{f_i - f_j}{L_f} \right)^2 \right] \equiv \sigma_b^2 C_{ij}, \tag{7}$$

where f is a field whose pattern represents that of the background error, which we call the error field. C_{ij} is the corresponding correlation coefficient. Eq. (**7**) formulates a covariance function which is positive definite according to the definition 2.2 in Gaspari and Cohn (Gaspari and Cohn 1999) and Schur product theorem (cf. Horn and Johnson 1985, p.458). In this study, *f* is chosen to be either the true error field of the background or a certain estimate of the true error. L_f is the de-correlation scale in the error field space in units of g kg^{-1} for our moisture retrieval experiments; it controls the degree of the anisotropy. The spatial covariance defined in Eq.(7) is larger between two nearby points with similar background errors. As a result, the spatial covariance pattern is stretched along the direction of *f* contours, and squeezed across the contours.

Equation (7) is based on the idea of Riishøjgaard (1998) with an important difference. In his work, it is suggested that the analysis background field be used as the *f*, under the assumption that the error field has a similar pattern as the background field. This may be true for certain quasi-conservative quantities that are advected by the flow, but not necessarily true for all fields. In our case, *f* is defined as the error field. To estimate the *f* field, one possibility is to first perform an isotropic analysis, then use the difference between this 'trial' analysis and the background as an estimate of the error field. This idea will be evaluated in our analysis experiments.

b. Recursive filter

As pointed earlier in Introduction, the explicit filters used in LX06 are computationally very expensive. The univariate 3DVAR analyses in LX06, using the explicit anisotropic filters

with L_r = 4 grid intervals and L_f = 2 g kg^{-1} together with the cutoff radii of 10 grid intervals in the horizontal and 6 coordinate layers in the vertical, typically require about 160 minutes of CPU time to perform 100 minimization iterations while it takes the recursive filter only about 4 minutes to do the same, using a single 1.1 GHz IBM Power 4 (Regatta p690) processor. The recursive filters are much more efficient because the filters are typically applied only once or a few times (in the case of multiple filter passes) in each filtering direction while the explicit filter is applied once at every grid point (see also Purser et al. 2003a for related discussions). For this reason, recursive filters, with an anisotropic option, are being implemented in a number of operational 3DVAR systems, including those at NCEP, for both global and regional analyses (Wu et al. 2002).

In LX06, the background error covariance, **B**, defined by Eq.(6) or Eq.(7) is directly evaluated and applied to the control variable in the form of an explicit filter. In this paper, the effect of **B** is realized through a recursive filter representation of the square root of **B**, or matrix **D** in Eq.(3), and the recursive filter is applied to control variable **v**. Purser *et al.* (2003a; b) describe the construction and application of numerical recursive filters for the task of synthesizing the background error covariances for variational analysis. Those two papers respectively deal with spatially homogeneous and isotropic, and spatially inhomogeneous and anisotropic covariances with recursive filters. Some important details on the filters are given below.

1) One dimensional recursive filter

The 3D filters can be created by the applications of multiple one-dimensional filters. The general nth-order one-dimensional recursive filter has two steps (Hayden and Purser 1995). First the advancing step:

$$q_i = \beta p_i + \sum_{j=1}^{n} \alpha_j q_{i-j}, \tag{8}$$

where p is the input and q is the output of the advancing step and n is the order of the recursive filter. Here, i is the grid point index and must be treated in increasing order so that the quantities on the right hand side of the equation are already known. The advancing step is followed by the backing step:

$$s_i = \beta q_i + \sum_{j=1}^{n} \alpha_j s_{i+j} \tag{9}$$

where s is the final output from the recursive filter and index i here must be treated in decreasing order. Parameters α_j are the filter coefficients and have the following relationship with β:

$$\beta = 1 - \sum_{j=1}^{n} \alpha_j, \tag{10}$$

in order that the homogeneous forms of these filters conserve the quantity being filtered.

We note here that when the above recursive filter is applied to a limited area domain, as in our case, special boundary treatment is needed which is discussed by Purser *et al.* (2003a) in the appendices. The recursive filter operations can be easily performed in the advancing step according to Eq.(8) and the backing step according to Eq.(9) once the filter coefficients (α and β) are determined. In this study, we use a fourth-order recursive filter which effectively models the explicit Gaussian filter with a single pass (Purser et al. 2003a). In our application, the input quantities p_i in Eq.(8) correspond to the elements of control variable **v** in Eq. (4).

2) 'Aspect tensor' and 'hexad' algorithm

For 3D problems, in the isotropic case, one simply applies three one-dimensional filters, one in each coordinate direction. In the anisotropic case, however, the background error pattern can be stretched or flattened in directions oblique to the alignment of the grid coordinates. The

covariance operator in the anisotropic case is constructed by applying six recursive filters along six directions corresponding, in general, to a special configuration or a 'hexad' of oblique lines of the grid. This hexad can be determined from an 'aspect tensor' which is defined to be the normalized centered second-moment of the response of the filter representing the desired covariance locally (see Eq. 12). It therefore serves as a convenient way of characterizing the local spatial structure of the covariance. The term goes beyond the concept of the 'aspect ratio', which only describes the ratio of vertical and horizontal scales in the simplest horizontally-isotropic case, because the tensorial character expresses not just the absolute scale, but the dominant shape components.

A so-called 'hexad algorithm' is used to determine from the aspect tensor the six filtering directions and the corresponding hexad 'weights', which are the squares of the six unidirectional scalar filtering scales. Each weight is, in effect, a one-dimensional aspect tensor, in grid space units, associated with the corresponding generalized grid line belonging to the hexad configuration. The algorithm is described briefly in Purser et al. (2003b) and in much greater technical detail in Purser (2005). While it is inappropriate to reconstruct the detailed technical description of the hexad algorithm here, it is important to note that the generic 'hexad' of lines is not any arbitrary set of six generalized grid lines; the rules for the construction of a legal hexad require that the smallest discrete steps, or 'generators', of the first three of a 'hexad's directions, expressed in grid units as integer 3-vectors, form a parallelepiped of unit volume. Furthermore, the remaining three lines' generators consist of the three distinct possible differences amongst the first three generators. By these rules, the six generators of a hexad, together with their negatives, collectively define the 12 vertices of a distorted 'cuboctahedron' embedded within the lattice of local grid displacements. As is shown rigorously in Purser (2005), these constitutive rules

defining a legal hexad, together with the assumption that the centered second moments of a sequence of filters combine additively, and the further reasonable stipulation that the hexad weights on which the aspect tensor is projected are each nonnegative, generally ensures a unique choice of a hexad of filtering directions and weights, apart from the vacuous ambiguity of directions in special transitional cases where one or more hexad weights vanish. (A negative weight would imply a negative amount of diffusion for a Gaussian smoother, which is physically meaningless, but a vanishing hexad weight simply implies the acceptable limiting case of no smoothing in that direction.).

In order to find the aspect tensor at each grid point for the flow-dependent background error covariance defined in Eq. (6), it is necessary to rewrite Eq. (6) in matrix and differential form. The finite difference $f_i - f_j$ in Eq. (6) is approximated by infinitesimal differential df and distance r_{ij} is replaced by the differential $d\mathbf{y}$, then we obtain

$$\mathbf{B} = \sigma_b^2 \exp\left[-\frac{1}{2}\left(\frac{d\mathbf{y}^T d\mathbf{y}}{L_r^2} + \frac{(df)^2}{L_f^2} \right) \right]. \tag{11}$$

This anisotropic background error correlation should shrink along the direction of strong gradient of the error field compared to the corresponding isotropic one. For example, if the gradient of the error field is large in a given direction, then the difference in the background errors is large, i.e., df is large, so that the background error correlation is small between points in that direction, according to Eq. (). Alternatively, the background error covariance can be written in a general Gaussian form that involves aspect tensor, $\mathbf{A}$, as follows,

$$\mathbf{B} = \sigma_b^2 \exp\left(-\frac{1}{2} d\mathbf{y}^T \mathbf{A}^{-1} d\mathbf{y} \right). \tag{12}$$

Equating Eq. () and Eq. (12) then gives

$$dy^T \mathbf{A}^{-1} dy = \frac{dy^T dy}{L_r^2} + \frac{(df)^2}{L_f^2}. \qquad (13)$$

Differentiating the above equation twice with respect to **y,** and making the assumption that second derivatives of f can be neglected, gives the inverse of **A** as follows,

$$\mathbf{A}^{-1} = \frac{\mathbf{I}}{L_r^2} + \frac{(\nabla f)^T (\nabla f)}{L_f^2}, \qquad (14)$$

where ∇f is the gradient vector of f field. For 3D problems, **I** is a 3×3 identity matrix in our case. Note that in the cases where different geometric length scales are used for the horizontal and vertical directions, term $\mathbf{I}/L_r^2$ in Eq. (14) should be a more general diagonal matrix. The aspect tensor **A** is a 3×3 symmetric and positive definite matrix and should have six independent components in general. It is locally defined at each grid point but is assumed to vary smoothly in space. Its linear projection onto the appropriate hexad's weights is therefore also a smooth function over the region of physical space to which that particular hexad configuration maps. When L_f goes to infinity, the anisotropic filter reduces to the special case of the isotropic one since, in this situation, the second term on the right side of Eq. (14) vanishes. The resulting diagonal matrix A must therefore map to a degenerate hexad in which three of the six weights vanish while the filtering that corresponds to the three nonvanishing weights acts only along the three coordinate directions. In this special situation, the effective filtering scale does not change with grid points when the geometric de-correlation scale, L_r, is constant.

c. Estimation of background error field for anisotropic analysis

The variable f in Eq. (6) represents the background error field. For simulated observations, we know the truth so the true background error is also known. We can use the true background error as f to obtain the aspect tensor **A** for flow-dependent background error

covariance according to Eq. (14). Then valid filtering directions and associated weights can be determined by the aspect tensor at each grid point. This is what will be done in experiment ANISO to be described in section 5b. But for realistic applications, the true background error is not known beforehand. In such a case, an estimate of the error is needed before we can perform any anisotropic analysis. Following LX06, we perform, first, an analysis using isotropic background error (as in an experiment called ISO). The difference between this analysis from the background is then used as an estimate of the background error field, i.e., as f in Eq. (6). An anisotropic analysis is then performed and this experiment is referred to as UB, implying 'Updated background error covariance **B**'. Such a two-step iterative approach is feasible in practice, and is in a sense a double-loop strategy that is similar in procedure to the double-loop approach commonly employed by operational systems of variational analysis (e.g., Courtier et al. 1994)

3. Generation of simulated observations

Simulated data will be used to test our analysis system in this study. With simulated data, both the atmospheric truth and the error properties of the observations are known. The Advanced Regional Prediction System (ARPS, Xue et al. 2000; 2001; 2003) in a generalized terrain-following coordinate is used to simulate the 3D water vapor field of a dryline case occurring at 20 UTC, June 19, 2002. The dryline is characterized by a strong moisture gradient. The generation of simulated observations is the same as in LX06. The true simulation is based on the configurations of CAPS (Center for Analysis and Prediction of Storms) real time forecast for IHOP (Xue et al. 2002). The analysis domain covers an area of 1620x1440 km^2 over the central Great Plains of the U.S. The ARPS 9-km simulation sub-sampled to the 36 km analysis grid is

considered the truth of the atmospheric water vapor field. Shown in Fig. 1 is the truth at the 5th terrain-following model level, or about 500 meters above the ground.

The following formula is used to simulate the GPS slant-path water vapor observations,

$$SWV_{ij} = \int_{i^{th}\ receiver}^{j^{th}\ satellite} q_v\ ds, \tag{15}$$

where SWV_{ij} is the integrated water vapor along the slant path between the ith ground-based receiver and the jth GPS satellite, and q_v is the specific humidity along the path, interpolated from the grid point values of the truth. As in LX06, the GPS observation network is composed of 9 irregularly distributed satellites and 132 ground-based receivers which are evenly distributed in the analysis domain. There is one receiver station every four grid points, giving a receiver network resolution of 144 km in each horizontal direction. Therefore, for our analysis grid, there are 1188 SWV observations and 132 surface observations. Figure 2 in LX06 gives a schematic illustration of the GPS observation network.

4. Single observation tests

To assess the performance of the variational method described above using recursive filters and, more importantly, to understand the behaviors of the isotropic and anisotropic recursive filters, two single-observation experiments are performed using two-dimensional isotropic and anisotropic recursive filters, respectively. In such experiments, the SWV observation term is excluded from the cost function. Only one moisture observation at the surface marked by a filled black dot in Fig. 2, with a value of 14.72 g kg^{-1}, is analyzed. The background is set to a constant value of zero and the geometric de-correlation filter scale L_r is specified as 4 grid intervals. Since the filters are two dimensional, there is no coupling between

the vertical levels therefore the analyses are essentially two dimensional. We will therefore examine the surface field only, which is impacted by the single surface observation.

Fig. 2 shows the surface analysis increments from these two experiments. Since the background is zero, the analysis increments are the analysis themselves and represent the corresponding structures of the background error covariance. Fig. 2a shows, as expected, the circular shape of the isotropic analysis increment. For the anisotropic case, L_r is also set to be equal to 4 grid intervals while L_f is specified as 2 g kg^{-1}. The 'true' moisture field is used as the reference field (error field f) for this analysis (the background is zero in this case). Strong anisotropy in the analysis increment is clearly revealed by Fig. 2b; the increment is stretched along the directions of the contours of the reference field. This is because the correlation decreases rapidly through the region where the reference field has a strong gradient, e.g., west of the single observation; in contrast, it decreases much more slowly near the northeast of the observation, where the gradient is small. The analyzed values at the observation station for both cases are about 14.69 g kg^{-1}, which is very close to the observed value 14.72 g kg^{-1}. This result is consistent with the given ratio, i.e., 1:500, of the weighting coefficients of the background and surface observation terms in the cost function; the analysis is much closer to the observation than to the background. In the current ideal case where the background error covariance is modeled after the known truth, using an anisotropic recursive filter, the analysis should match the truth very well when a sufficient number of observations are present. This will be examined in the next section.

5. Three-dimensional moisture analysis

The earlier single-observation experiments demonstrate correct behaviors of our analysis system using recursive filters. Subsequently, we move to the analysis of full 3D water vapor field

from simulated *SWV* and surface moisture observations discussed in section 3. Three experiments are discussed in this section, which use different background error covariances. In all three cases, the observational data are error-free, and the analysis background was created by smoothing the truth 50 times, using a 2-D horizontal 9-point filter. Our main purpose in this study is to examine the ability of our 3DVAR system to analyze meso- and small-scale moisture structures from the *SWV* and surface observations with an initial guess that does not contain such structures. The background produced by smoothing truth is adequate for this purpose. Example horizontal and vertical cross-sections of this smoothed field can be found in Fig. 4 of LX06.

In the first experiment, called ISO (Table 1), the correlation between any two points is only a function of their distance, so the covariance is isotropic; it is modeled using the isotropic recursive filter. The covariance is also assumed to be spatially homogeneous. For the latter two experiments, the correlation is the function of not only the distance but also the error structure; the covariance is therefore state-dependent (or flow-dependent) and is modeled using an anisotropic recursive filter. For the first of the two, called ANISO (Table 1), the error field is based on the truth field, i.e., the *f* in Eq. (6) is equal to the truth minus analysis background. Through this experiment we can determine how well our analysis system can recover the 3D humidity field from the *SWV* and surface moisture observations under an ideal condition. For the second of the two anisotropic experiments (called UB, Table 1), the iterative procedure described in section 2c is employed, in which an estimate of the error field, as the difference between the first isotropic analysis and the background, is used for the subsequent anisotropic analysis.

a. Analysis with an isotropic background error covariance model

The one-dimensional fourth-order isotropic recursive filter is applied along each coordinate direction using one pass only (Purser et al. 2003a). The horizontal and vertical

filtering scales are chosen to be four grid intervals which are found to be nearly optimal for this case (see later discussion in subsection 6a). The choices of the geometric part of the filtering scales are, in practice, often linked to the observational network density; we want the observation innovation spreads far enough so that it at least covers the gaps between ground receiver stations (in the current case the station spacing is 4 grid intervals). The sensitivity of the analysis to the value of the de-correlation length scale is examined in subsection 6a.

Figure 3 shows the cost function and the norm of the cost-function gradient as functions of the number of iterations during the minimization procedure for experiment ISO. Significant reductions (by at least two orders of magnitude) occur in both the cost function and the norm of the gradient during the first 100 iterations. In all cases, we run the minimization algorithm for 100 iterations, which should be sufficient for the desired accuracy.

Shown in Fig. 4 is the east-west vertical cross-section of the analyzed 3D water vapor field (dashed lines) versus the truth of the moisture field (solid lines) at $y = 270$ km (along A-B line in Fig. 1). It can be seen that the analysis follows the truth reasonably well. The moisture contours take an essentially vertical orientation at the location of the dryline (about $x = 360$ km) below the 1.5 km level. This boundary separates the dry air from the high plateau to the west and the moist air originating from the Gulf of Mexico to the east. Moisture ridges and troughs are found at the right locations and the moisture extremum centers match the truth well also.

This analysis obtained using an isotropic recursive filter is actually much better than that obtained using an explicit isotropic Gaussian filter (c.f., Fig. 7 in LX06). All parameter configurations are the same as experiment SNF in LX06 except for the geometric de-correlation scale L_r, which was set to 3 grid intervals that was found to be optimal for that case. In the case of explicit filtering, the correlation had to be cut off at a certain distance to keep the

computational cost manageable. This action actually destroys the exact positive definiteness of the background error covariance[1] although the effect is usually small. In the case of the recursive filter, no cut-off radius is necessary so that the positive definite property can be preserved. In addition, the recursive filter does have the important advantage of being much more computationally efficient than the explicit filter.

The analysis increment at the 5th model level is presented in Fig. 5a, together with the corresponding truth increment (truth minus background) in Fig. 5b. They show roughly similar patterns and extremum locations. The dryline can be recognized easily in the analysis. The overall correlation coefficient (CC) and the root-mean square error (RMSE) between the analysis increment and the truth increment are presented in Table 1. The CC is 0.84 and the RMSE is 0.35 g kg^{-1}, both indicating good analysis. For reference, the RMSE for the background is 2.70 g kg^{-1}.

b. Analysis with an anisotropic background error covariance model

Experiment ANISO is performed to examine how the anisotropic background error covariance affects the analysis. The chosen de-correlation scales are four grid intervals for L_r and 2 g kg^{-1} for L_f. This set of scales will be shown to be nearly optimal in section 6a. The analysis increment at the 5th grid level shown in Fig. 6a matches the truth increment (Fig. 5b) very well. The dryline pattern is analyzed with pronounced similarity to the truth. Their extremum locations coincide almost exactly. The analysis through the same vertical cross section as in Fig. 4 is shown in Fig. 6b. Obviously, there is a significant improvement compared to the analysis of ISO. The dryline structure is analyzed very well and the analyzed moisture contours almost coincide with the truth. The fine-scale structures are also captured well. For example, the $q_v = 14.0$ g kg^{-1}

---

[1] Gaspari and Cohn (1999) have proposed filter functions for localizing covariance while preserving the positive definiteness. These functions can be applied to the explicit filter although they do not solve the problem we have with an anisotropic explicit filter.

contour has a sharp downward drop at x = 620 km in the truth, a fine-scale feature that is also captured by the analysis. Further, an upward moisture bulge at x = 300 km, associated with upward motion at the dryline, is recovered very well by this anisotropic analysis but is missed in the isotropic analysis. The overall CC and RMSE for experiment ANISO are, respectively, 0.91 and 0.28 g kg^{-1} (Table 1), obviously better than those of ISO.

c. Anisotropic analysis based on estimated background error field

Experiment ANISO presented in the previous subsection has shown clearly that the use of an anisotropic spatial filter improves the results of analysis when the background error covariance is modeled based on the structure of true error field. This suggests that flow-dependent background error covariance can play a significant role in 3DVAR system. However, in reality, the true error field is not known beforehand. One promising solution is to use an ensemble of forecasts to estimate the flow-dependent error covariances (e.g., Buehner 2005) but the cost of running the ensemble is high. Here, we present results from experiment UB, which has been introduced earlier in this section and also discussed in section 2c and uses a two-step iterative procedure.

The analysis of UB is shown in Fig. 7. The analysis increment at the 5th grid level (Fig. 7a) is more stretched along the dryline direction in comparison with the analysis from ISO (Fig. 5a), and the pattern also agrees with that of the true increment (Fig. 5b) much better. The agreement of the analysis with the truth is also excellent in the vertical cross section (Fig. 7b). For example the 4 and 6 g kg^{-1} q_v contours match the truth contours down to the fine scale details while the fine-scale details of the ISO analysis are not as good (Fig. 4). These fine-scale structures may play an important role for accurate convective initiation along a dryline and the subsequent precipitation forecast. The CC and RMSE for this experiment are 0.86 and 0.34 g kg^{-}

[1], respectively, compared to the 0.84 and 0.35 g kg^{-1} of ISO. The improvement, though not as dramatic as ANISO, is nevertheless evident. This improvement is in fact more evident in the analyzed fields shown in Fig. 7 than these scores reveal.

To provide a quantitative measure of the difference between the flow-dependent **B** derived from the 'updated' error field (i.e., the 'updated' **B** used in experiment UB) and that derived from the true error field (i.e., the 'truth-based' **B** used in experiment ANISO), we calculate the L2-norm of the difference (matrix) between the two matrices. It is found that this difference is a factor of 2.5 smaller than that between the truth-based **B** and the isotropic **B** (i.e., the **B** used in experiment ISO), indicating that the updated **B** is much closer to the truth-based **B** than the isotropic one.

The above procedure for estimating **B** is an iterative procedure. One naturally would ask if additional iterations would further improve the estimation of **B** and the subsequent analysis. To seek the answer, additional iterations were performed. It was found that the quality of analysis after the third iteration remains essentially the same, therefore only one update step or two total iterations are employed here. This result may be case dependent, however. It should be tested when applying it to other cases.

6. Sensitivity experiments

a. Sensitivity to de-correlation scales

The quality of an analysis is closely related to the de-correlation scales used in Eqs. (5) and (6); these scales control the spatial extent over which an observation increment is spread. Fixed values of L_r (4 grid intervals) and L_f (2 g kg^{-1}) were used in the earlier 3D moisture analysis experiments. We examine in this subsection how the analysis quality varies with the de-correlation scales, as measured by the CC and RMSE of the analysis increment with the true

increment. In these sensitivity experiments, the weighting coefficients specified for the terms in the cost function remain the same.

In the isotropic case, only L_r is a free parameter. Given that the truth of moisture is known, we can explore the parameter space of L_r in order to find a value that yields the best moisture analysis. In Fig. 8, the dotted line shows the RMSEs of analysis as a function of L_r (in units of analysis grid intervals). We see that the optimal de-correlation length scale is equal to four grid intervals for this isotropic case. This appears reasonable because the 4 grid interval is actually the distance between our uniformly spaced ground receivers.

In the anisotropic case, there are two free parameters, L_r and L_f, so we explore the parameter space of the correlation model to find the set of L_r and L_f that yields the best analysis. For the experiments that use 'updated' **B,** the RMSEs (solid lines in Fig. 8) as a function of L_r are presented for four different values of L_f, that is, 1, 2, 3 and 4 g kg^{-1}. It can be seen that for the L_f = 1 g kg^{-1} case, the RMSEs are the largest among all cases when $L_r \leq 4$ grid intervals. This suggests that this value of L_f is too small when L_r is also small, so that the combined spatial correlation fails to fill the gaps between observation stations. For other more appropriate values of L_f, the optimal value of L_r is 4 grid intervals. Overall, the optimal de-correlation scale set is L_r = 4 grid intervals and L_f = 3 g kg^{-1} for the 'updated' **B** cases.

The dashed line in Fig. 8 shows the RMSEs as a function of L_r, for experiments that use the **B** based on that the true error field. ANISO is one of the experiments. L_f is equal to 2 g kg^{-1} for these experiments. It is obvious that this set of experiments always yields the best analysis for a given value of L_r, compared to the other sets of experiments. It is also clear from Fig. 8 that when $L_r \geq 4$ the isotropic analysis is always worse than the corresponding anisotropic analyses with the same L_r, except for the anisotropic case with 'updated' **B** and L_f = 1 g kg^{-1}. For $L_r \leq 3$, the

analyses are of similar quality except for the $L_f = 1$ g kg^{-1} case. As pointed out earlier, this value of $L_f = 1$ g kg^{-1} is too small. The RMSE increases considerably with L_r when it is larger than 4 grid intervals for the isotropic case whereas the worsening is much less significant for the anisotropic cases, indicating a much smaller sensitivity of the analysis to the choice of L_r in the anisotropic cases; the use of an improperly large L_r that helps to fill the observation gaps does not hurt as much as the isotropic case. This is because in the anisotropic case, the field-dependent covariance imposes an additional constraint on the spatial spread of the observation increment, and helps limit the potential damage of too large an L_r. As long as the choice of L_f is appropriate, the analysis tends to be good, according to Fig. 8.

b. Sensitivity to typical observation errors

All experiments presented so far use simulated *SWV* and surface moisture data that include no observation errors. In practice, the observations would not be error-free, so it is important to test the sensitivity of the analysis to the observation errors, in part to test the robustness of our analysis system. We perform experiment UB_err, which is the same as experiment UB except for the errors added to the observations. The standard deviations added to the simulated surface and *SWV* observations are, respectively, 5% and 7% of the error-free values and the added errors are normally distributed with zero means. The *SWV* errors are consistent with the estimate of Braun et al. (2001) for real data. In this case, because of the presence of observation errors, the weighting coefficients for *SWV* and surface observation terms are specified to 15 and 29, respectively, relative to the 1 of the background term. These weights are specified to be proportional to the inverse of estimated background error variance and the variances of the errors added to simulated observations (see discussion section 3a). The analysis from this experiment, though not as good as the corresponding error-free case, still matches the

truth reasonably well (Fig. 9). In other words, our 3DVAR analysis procedure is able to retrieve the 3D structure of moisture field from the slant-path water vapor observations (which are integrated values), even though the observations are contaminated by errors of typical magnitudes. This is also supported by the error statistics. The overall correlation coefficient of the increments decreases from the 0.84 of the error-free UB case to 0.80 and the RMSE increases from 0.35 g kg^{-1} to 0.42 g kg^{-1} (Table 1).

7. Conclusions

Compared to Liu and Xue (2006) which uses an explicit spatial filter, a computationally much more efficient algorithm based on the recursive filter is implemented and evaluated in this study, for the purpose of analyzing three-dimensional water vapor fields from simulated GPS *SWV* observations. Surface moisture observations collected at the ground receiver sites are analyzed at the same time. This study represents the first time that a fully anisotropic recursive filter is used for modeling flow-dependent background errors in the context of analyzing GPS observations. The main conclusions are listed as follows.

1) The analysis, produced by our 3DVAR method with an isotropic recursive filter, captures the main structure of the dryline examined.

2) An anisotropic recursive filter, which is adaptive to the structure of the background error both in smoothing directions and spatial correlation scales, produces significantly better analyses of the specific humidity field associated with a dryline than the isotropic one, especially in the fine-scale moisture structures.

3) In the absence of a good knowledge of the background error, a two-step iterative procedure for its estimation is proposed, in which an isotropic analysis is performed first. The difference between this tentative analysis and the background is used to define the error field

needed by the flow-dependent background error covariance model. This estimated error field is then used in the second anisotropic analysis step. Improved analysis, compared to the isotropic one, is obtained through this procedure.

4) Experiments on the sensitivities of the analysis to the error de-correlation scales are performed. It is found that the isotropic analysis is more sensitive to the geometric de-correlation scale L_r and in such a case the range of L_r with which a good analysis is obtained is narrow. When the flow-dependent component of the background error is introduced, the analysis becomes much less sensitive to L_r. For the current dryline test case, the optimal geometric length scale L_r is found to be roughly equal to the mean distance between the GPS ground receiver stations.

5) The analysis procedure is found to be feasible and effective for this dryline case. The analysis is found to be not very sensitive to the presence of observational errors of typical magnitudes in the *SWV* data and in the surface moisture observations. But more sensitivity tests are necessary to show the statistical significance and general applicability of this finding.

6) Compared to the explicit filters examined in Liu and Xue (2006), the biggest advantage for using recursive filters is the computational efficiency. The computational cost of a recursive filter is about 40 times smaller than that of the corresponding explicit filter even when moderate cut-off radii are used. The quality of analyses using recursive filters are in general comparable to the analyses obtained with explicit filters. In the isotropic case, the analysis obtained using the recursive filter is actually better than that of the explicit filter.

Here, we point out that because the formulation of the background term is the same in 3DVAR and 4DVAR, our method can be applied to 4DVAR as well. The application of recursive filters to 4DVAR is exactly analogous to, though somewhat more complicated than, the

application to 3DVAR. Purser (2005) briefly describes the construction of fully 4D anisotropic covariance operators via the sequences of line filters that generalize the sequences obtained through the hexad method.

In the near future, we will use the retrieved moisture field to initialize a mesoscale model, such as the ARPS, and to examine the impact of assimilating *SWV* data on short-range precipitation forecasts. The assimilation and the examination of the impact of real *SWV* data collected during the IHOP_2002 field experiment are also planned. The results of this current study can be statistically more significant if the procedure tested against more cases. Further, the effectiveness of the two-step procedure for estimating the background error, then using it in the analysis, is worth further investigation as it is applied to more cases.

Acknowledgement

References

Braun, J., C. Rocken, and R. Ware, 2001: Validation of line-of-sight water vapor measurements with GPS. *Radio Sci.*, **36,** 459-472.

Buehner, M., 2005: Ensemble-derived stationary and flow-dependent background-error covariances: Evaluation in a quasi-operational NWP setting. *Quart. J. Roy. Meteor. Soc.*, **131,** 1013-1043.

Courtier, P., J.-N. Thépaut, and A. Hollingsworth, 1994: A strategy for operational implementation of 4D-Var, using an incremental approach. *Quart. J. Roy. Meteor. Soc.*, **120,** 1367-1387.

Cucurull, L., F. Vandenberghe, D. Barker, E. Vilaclara, and A. Rius, 2004: Three-dimensional variational data assimilation of ground-based GPS ZTD and meteorological observations during the 14 December 2001 storm event over the western Mediterranean Sea. *Mon. Wea. Rev.*, **132,** 749-763.

De Pondeca, M. S. F. V. and X. Zou, 2001a: Moisture retrievals from simulated zenith delay "observations" and their impact on short-range precipitation forecasts. *Tellus*, **53A,** 192-214.

De Pondeca, M. S. F. V. and X. Zou, 2001b: A case study of the variational assimilation of GPS zenith delay observations into a mesoscale model. *J. Appl. Meteor.*, **40,** 1559-1576.

Falvey, M. and J. Beavan, 2002: The impact of GPS precipitable water assimilation on mesoscale model retrievals of orographic rainfall during SALPEX'96. *Mon. Wea. Rev.*, **130,** 2874-2888.

Gaspari, G. and S. E. Cohn, 1999: Construction of correlation functions in two and three dimensions. *Quart. J. Roy. Meteor. Soc.*, **125,** 723-757.

Guo, Y.-R., Y.-H. Kuo, J. Dudhia, D. Parsons, and C. Rocken, 2000: Four-dimensional variational data assimilation of heterogeneous mesoscale observations for a strong convective case. *Mon. Wea. Rev.*, **128,** 619-643.

Ha, S.-Y., Y.-H. Kuo, Y.-R. Guo, and G.-H. Lim, 2003: Variational assimilation of slant-path wet delay measurements from a hypothetical ground-based GPS network. Part I: Comparison with precipitable water assimilation. *Mon. Wea. Rev.*, **131,** 2635-2655.

Hayden, C. M. and R. J. Purser, 1995: Recursive filter objective analysis of meteorological fields: applications to NESDIS operational processing. *J. Appl. Meteor.*, **34,** 3-15.

Horn, R. A. and C. R. Johnson, 1985: *Matrix analysis*. Cambridge University Press, 561 pp.

Huang, X.-Y., 2000: Variational analysis using spatial filters. *Mon. Wea. Rev.*, **128,** 2588-2600.

Ide, K., P. Courtier, M. Ghil, and A. Lorenc, 1997: Unified notation for data assimilation: Operational, sequential and variational. *J. Meteor. Soc. Japan*, **75,** 181-189.

Kalnay, E., 2002: *Atmospheric modeling, data assimilation, and predictability*. Cambridge University Press, 341 pp.

Kuo, Y.-H., Y.-R. Guo, and E. R. Westerwater, 1993: Assimilation of precipitable water measurements into a mesoscale numerical model. *Mon. Wea. Rev.*, **121,** 1215-1238.

Kuo, Y.-H., X. Zou, and Y. R. Guo, 1996: Variational assimilation of precipitable water using a nonhydrostatic mesoscale adjoint model. Part I: Moisture retrieval and sensitivity experiments. *Mon. Wea. Rev.*, **124,** 122-147.

Liu, D. C. and J. Nocedal, 1989: On the limited memory BFGS method for large scale optimization. *Math. Programming*, **45,** 503-528.

Liu, H. and M. Xue, 2006: Retrieval of moisture from slant-path water vapor observations of a hypothetical GPS network using a three-dimensional variational scheme with anisotropic background error. *Mon. Wea. Rev.*, **134,** 933–949.

MacDonald, A. E., Y. Xie, and R. H. Ware, 2002: Diagnosis of three-dimensional water vapor using a GPS network. *Mon. Wea. Rev.*, **130,** 386-397.

Parrish, D. F. and J. C. Derber, 1992: The National Meteorological Center's spectral statistical-interpolation analysis system. *Mon. Wea. Rev.*, **120,** 1747-1763.

Pu, Z.-X., E. Kalnay, D. Parrish, W. Wu, and Z. Toth, 1997: The Use of bred vectors in the NCEP global 3D variational analysis system. *Wea. Forecasting*, **12,** 689-695.

Purser, R. J., 2005: A geometrical approach to the synthesis of smooth anisotropic covariance operators for data assimilation. NOAA/NCEP Office Note 447 (Available from NCEP, 5200 Auth Road, Camp Springs, MD 20746-4304), 60 pp.

Purser, R. J., W.-S. Wu, D. F. Parrish, and N. M. Roberts, 2003a: Numerical aspects of the application of recursive filters to variational statistical analysis. Part I: Spatially homogeneous and isotropic Gaussian covariances. *Mon. Wea. Rev.*, **131,** 1524-1535.

Purser, R. J., W.-S. Wu, D. F. Parrish, and N. M. Roberts, 2003b: Numerical aspects of the application of recursive filters to variational statistical analysis. Part II: Spatially inhomogeneous and anisotropic general covariances. *Mon. Wea. Rev.*, **131,** 1536-1548.

Riishøjgaard, L. P., 1998: A direct way of specifying flow-dependent background error correlations for meteorological analysis systems. *Tellus*, **50A,** 42-57.

Rocken, C., R. H. Ware, T. van Hove, F. Solheim, C. Alber, J. Johnson, M. Bevis, and S. Businger, 1993: Sensing atmospheric water vapor with global positioning system. *Geophys. Res. Lett.*, **20,** 2631-2634.

Ware, R., C. Alber, C. Rocken, and F. Solheim, 1997: Sensing integrated water vapor along GPS ray paths. *Geophys. Res. Lett.*, **24,** 417-420.

Weckwerth, T. M., D. B. Parsons, S. E. Koch, J. A. Moore, M. A. LeMone, B. B. Demoz, C. Flamant, B. Geerts, J. Wang, and W. F. Feltz, 2004: An overview of the International H2O Project (IHOP_2002) and some preliminary highlights. *Bull. Amer. Meteor. Soc.*, **85,** 253-277.

Wu, W.-S., R. J. Purser, and D. F. Parrish, 2002: Three-dimensional variational analysis with spatially inhomogeneous covariances. *Mon. Wea. Rev.*, **130,** 2905-2916.

Xue, M., K. K. Droegemeier, and V. Wong, 2000: The Advanced Regional Prediction System (ARPS) - A multiscale nonhydrostatic atmospheric simulation and prediction tool. Part I: Model dynamics and verification. *Meteor. Atmos. Physics*, **75,** 161-193.

Xue, M., D.-H. Wang, J.-D. Gao, K. Brewster, and K. K. Droegemeier, 2003: The Advanced Regional Prediction System (ARPS), storm-scale numerical weather prediction and data assimilation. *Meteor. Atmos. Physics*, **82,** 139-170.

Xue, M., K. Brewster, D. Weber, K. W. Thomas, F. Kong, and E. Kemp, 2002: Realtime storm-scale forecast support for IHOP 2002 at CAPS. *Preprint, 15th Conf. Num. Wea. Pred. and 19th Conf. Wea. Anal. Forecasting*, San Antonio, TX, Amer. Meteor. Soc., 124-126.

Xue, M., K. K. Droegemeier, V. Wong, A. Shapiro, K. Brewster, F. Carr, D. Weber, Y. Liu, and D.-H. Wang, 2001: The Advanced Regional Prediction System (ARPS) - A multiscale nonhydrostatic atmospheric simulation and prediction tool. Part II: Model physics and applications. *Meteor. Atmos. Phy.*, **76,** 143-165.

List of Figures

Fig. 6. (a) Analysis increment of q_v at the 5th grid level from experiment ANISO with contour

interval 1 g kg^{-1}, where dashed lines are for negative values and solid lines for positive

values. (b) East-west vertical cross-section of q_v at y = 270 km with interval 2 g kg^{-1}.

Solid lines are for truth and dashed lines for experiment ANISO.

Fig. 7. Same as in Fig. 6 but for experiment UB.

Fig. 8. The overall RMSE (g kg^{-1}) between retrieved 3D analysis increments and the true

increment (truth minus background), as a function of the geometric de-correlation scale

L_r (in units of analysis grid intervals). The dotted line is for the experiments using the

isotropic recursive filters (with ISO as one of them) and the dashed line is for the

experiments using the truth-based anisotropic background error covariance (with ANISO

as an example) with L_f = 2 g kg^{-1}. The solid lines are for the experiments with the

anisotropic error covariances based on the 'updated' error fields (e.g., UB) with L_f = 1, 2,

3, 4 g kg^{-1}, respectively.

Fig. 9. Same as in Fig. 6 but for experiment UB_err.

Fig. 1. The specific humidity, q_v, at the 5th terrain-following grid level, or about 500 meters above the ground, from ARPS 'truth' simulation for an IHOP case valid at 20 UTC, 19 June, 2002. The contour interval is 1 g kg^{-1}. The analysis domain is 1620 km x 1440 km in Great Plain. The dryline is represented by the strong gradient of q_v. The thick line A-B is at y = 270 km.
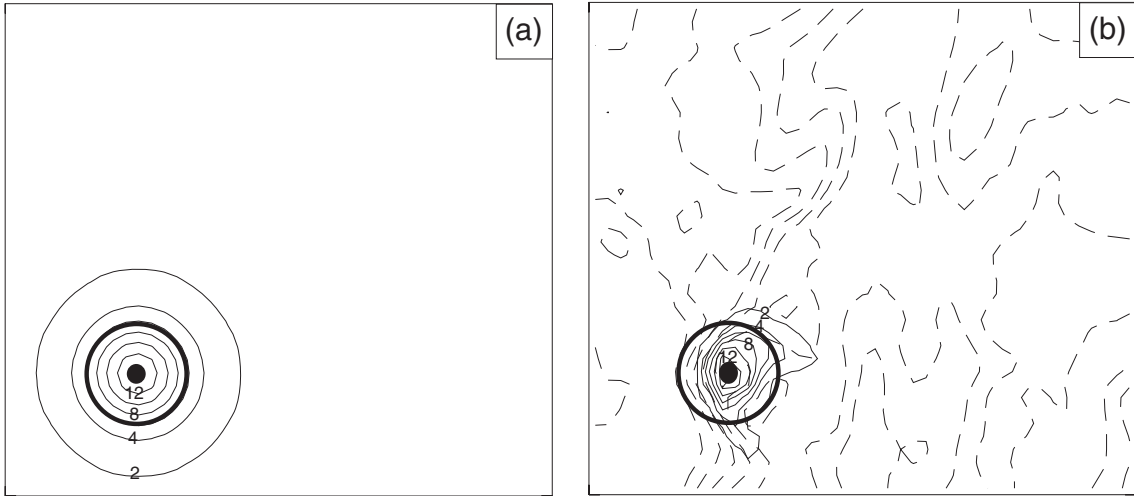
Fig. 2. Surface analysis increments from single observation experiments (a) for the isotropic example whose analysis increment is of circular shape and (b) for anisotropic example coupled to a reference field (dashed lines). The increment in the latter case is stretched along the contours of the reference field showing the strong anisotropy of the analysis. The contour interval for the increment is 2 g kg^{-1} and the first contour shown is at 2 g kg^{-1}. The filled black dots mark the locations of the single observations. A circle of radius $L_r = 4$ grid intervals and centered at the observation station is overlaid in thick black line in both panels.
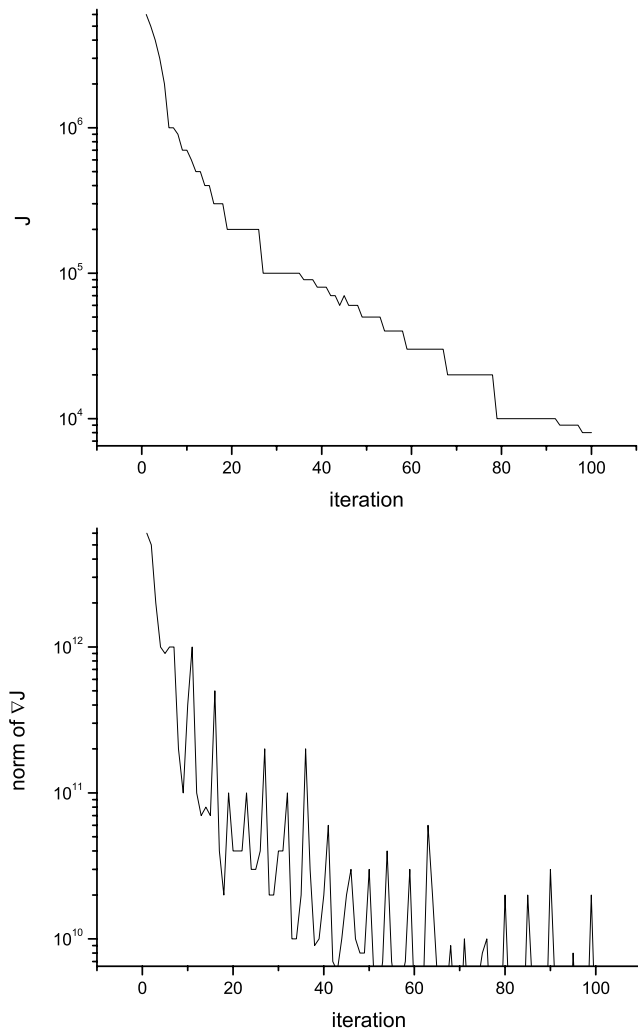
Fig. 3. The variation of the cost function J and the norm of the gradient ∇J with the number of iterations during the minimization procedure for experiment ISO.
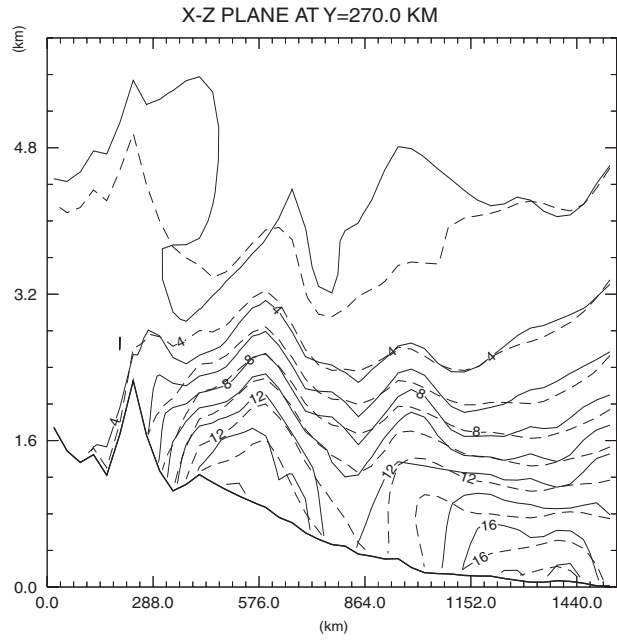
Fig. 4. East-west vertical cross-section of the retrieved specific humidity field (dashed lines) from experiment ISO at y = 270 km versus the truth (solid lines). The contour interval is 2 g kg^{-1}.
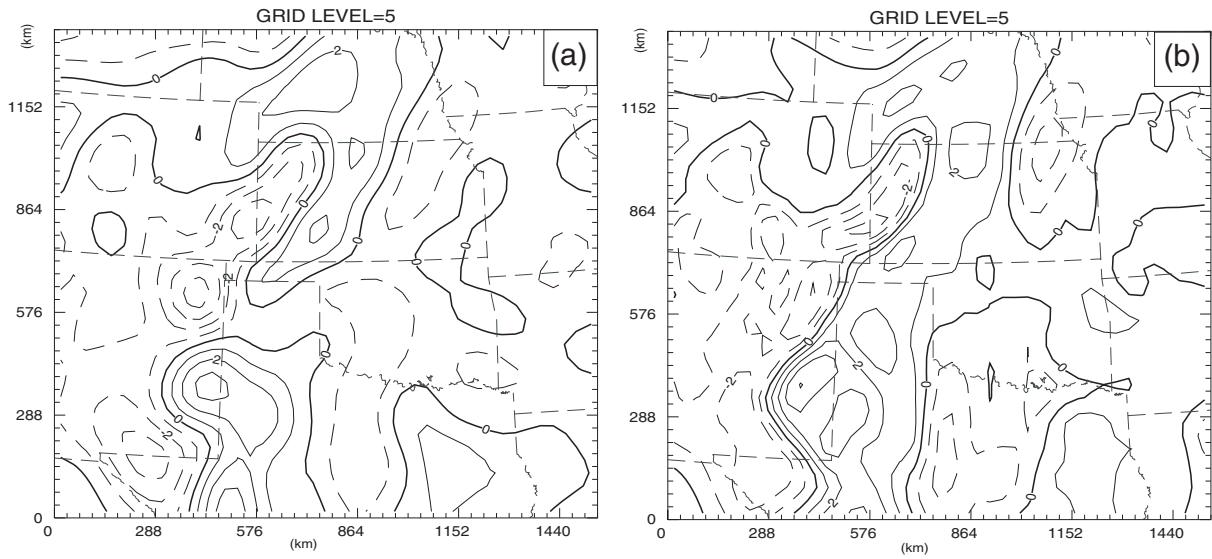
Fig. 5. (a) Analysis increment of q_v at the 5th grid level from the experiment ISO. (b) Truth minus background at the same level. The contour interval is 1 g kg^{-1}. Dashed lines represent negative values and solid lines positive values.
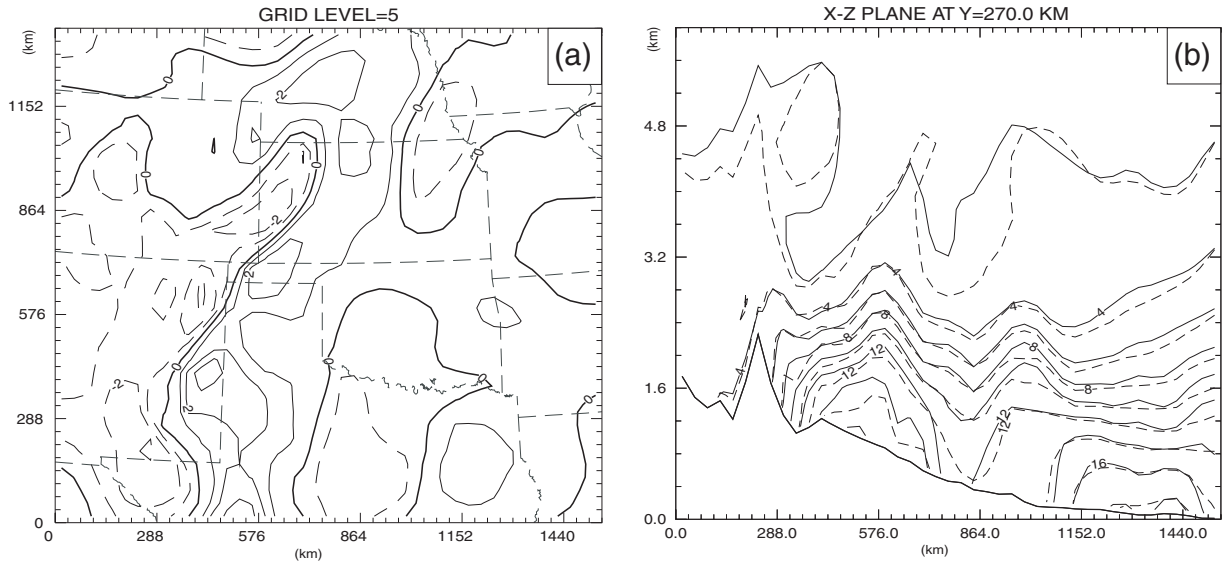
Fig. 6. (a) Analysis increment of q_v at the 5th grid level from experiment ANISO with contour interval 1 g kg^{-1}, where dashed lines are for negative values and solid lines for positive values. (b) East-west vertical cross-section of q_v at y = 270 km with interval 2 g kg^{-1}. Solid lines are for truth and dashed lines for experiment ANISO.
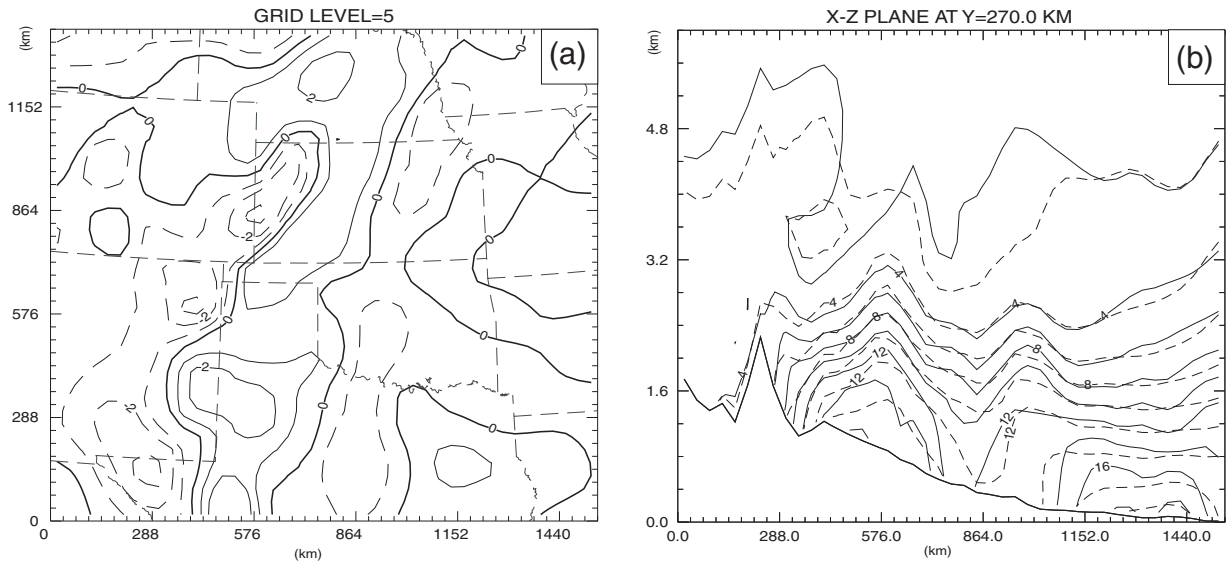
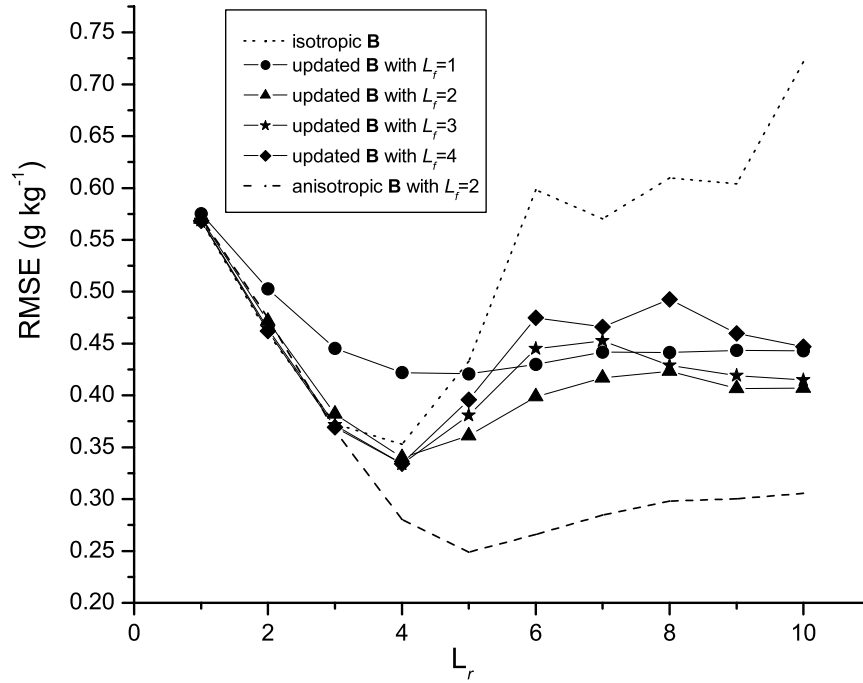Fig. 7. Same as in Fig. 6 but for experiment UB.

Fig. 8. The overall RMSE (g kg^{-1}) between retrieved 3D analysis increments and the true increment (truth minus background), as a function of the geometric de-correlation scale L_r (in units of analysis grid intervals). The dotted line is for the experiments using the isotropic recursive filters (with ISO as one of them) and the dashed line is for the experiments using the truth-based anisotropic background error covariance (with ANISO as an example) with $L_f = 2$ g kg^{-1}. The solid lines are for the experiments with the anisotropic error covariances based on the 'updated' error fields (e.g., UB) with $L_f = 1, 2, 3, 4$ g kg^{-1}, respectively.
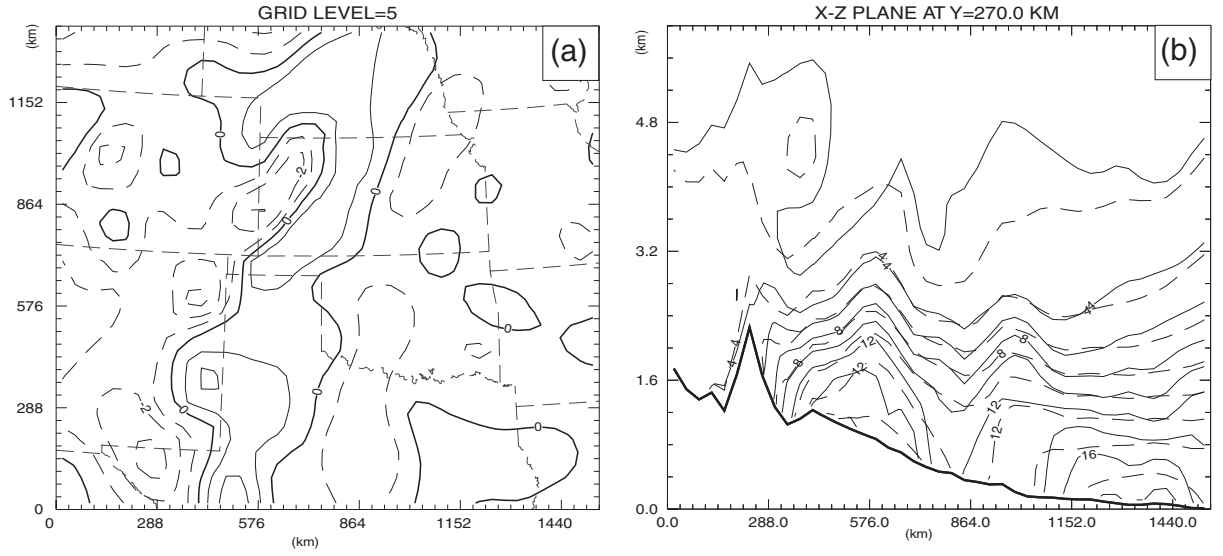
Fig. 9. Same as in Fig. 6 but for experiment UB_err.

Table 1. List of retrieval experiments. In this table, *SWV* denotes GPS slant-path water vapor data and 'sfc' denotes the surface moisture observation data. CC is the overall correlation coefficient and RMSE is the root-mean square error between the derived moisture increment and the true moisture increment (truth minus background).

Experiment	Observational errors	anisotropic Filter	RMSE (g kg^{-1})	CC	CC in LX06
ISO	No	No	0.35	0.84	0.83[*]
ANISO	No	Yes	0.28	0.91	0.93
UB	No	Yes	0.34	0.86	0.83
UB_err	5% sfc error 7% *SWV* error	Yes	0.42	0.80	0.79

[*] *L_r = 4, in unit of grid point, which is optimal, for ISO experiment in this study while L_r = 3 is optimal in LX06.*